Contents lists available at ScienceDirect

Energy Conversion and Management

journal homepage: http://ees.elsevier.com

# Advanced concept of coupling solar-aided flue gas treatment and solar-aided power generation in power plants

Yu-Hang Yu [a,b], Shao-Peng Guo [d], Yong Hao [b,c], Mao-Bin Hu [a], Rui-Lin Wang [b,c]

[a] School of Engineering Science, University of Science and Technology of China, Hefei 230026, China
[b] Institute of Engineering Thermophysics, Chinese Academy of Sciences, Beijing 100190, China
[c] University of Chinese Academy of Sciences, Beijing 100049, China
[d] School of Energy and Environment, Inner Mongolia University of Science and Technology, Baotou 014010, China

ARTICLE INFO

*Keywords*
Solar-aided flue gas treatment
Solar-aided power generation
Nitric oxide decomposition
Improved flue gas treatment sequence
Flue gas feed water preheating

ABSTRACT

In this paper, an advanced concept of coupling solar-aided flue gas treatment (SAGT) and solar-aided power generation (SAPG) is proposed to realize the low energy consumption flue gas treatment for fossil fuel power generation systems. An improved flue gas treatment sequence outside boilers is proposed in SAGT, where denitration is configured downstream of flue gas desulfurization (FGD). By using a parabolic trough collector (PTC) solar field, flue gas can be heated up to 550 °C in the collectors. The treatment sequence therefore can be achieved with the assistance of solar field. Finally, the waste heat of flue gas is utilized to preheat the feed water of boilers to enhance the power generation of power plants. A 600 MW coal-fired power plant system is analyzed as a case study. The calculation results show that SAGT and SAPG have relatively good performances both on stability and solar-to-electricity efficiency. This study might provide a new solution to deal with the difficulties of treating flue gas inside boilers such as deactivation and blockage of catalysts. Furthermore, efficient utilization of solar energy realizes both environment protection and energy conservation.

**Nomenclature**

| | |
|---|---|
| $\widetilde{G}_{NO}$ | The mass of NO (kg/kg coal) |
| $\widetilde{N}_{TA}$ | The amount of substance of theoretical air (mol/kg coal) |
| $\widetilde{n}_{NOx}$ | The amount of substance of $NO_x$ (mol/kg coal) |
| $\widetilde{n}_{CO_2}$ | The amount of substance of $CO_2$ (mol/kg coal) |
| $\widetilde{n}_{O_2}$ | The amount of substance of $O_2$ (mol/kg coal) |
| $\widetilde{n}_{N_2}$ | The amount of substance of $N_2$ (mol/kg coal) |
| $q_f$ | The low heating value of the raw anthracite (kJ/kg) |
| $\theta$ | Incident angle (°) |
| $\beta$ | The conversion rate of nitrogen to NO in fuel (%) |
| $\beta_{cov}$ | The conversion rate of decomposing NO (%) |
| $c_{NO,\,0}$ | The initial concentration of NO (mol/m$^3$) |
| $c_{NO}$ | The concentration of NO (mg/Nm$^3$) |
| $P_{reac}$ | The pressure of flue gas in reactor (Pa) |
| $T_{reac}$ | The temperature of flue gas in reactor (K) |
| $r_{NO}$ | Reaction rate of NO (mol/(m$^3$·s)) |
| $\tau$ | The residence time or reaction time (s) |
| $k_{app}$ | The apparent rate constant (-) |
| $K_\alpha$ | The equilibrium constant (-) |
| $\dot{Q}_{abs}$ | The thermal energy absorbed by flue gas (W) |
| $\varphi_{NO,\,0}$ | The initial volume fraction of NO (%) |
| $I$ | Direct normal irradiation (W/m$^2$) |
| $T_{ave}$ | Average temperature of solar field (K) |
| $T_{sfield,\,i}$ | Temperature of flue gas in the inlet of solar field (K) |
| $T_{sfield,\,o}$ | Temperature of flue gas in the outlet of solar field (K) |
| $\dot{m}_{ms}$ | The mass flow rate of the main steam (kg/s) |
| $\dot{m}_{rh}$ | The mass flow rate of reheat steam (kg/s) |
| $\dot{m}_{coal}$ | The consumption rate of coal (kg/s) |
| $\widetilde{h}_{fg}$ | The enthalpy of flue gas (kJ/kg coal) |
| $\Delta\widetilde{h}_{fg,n}$ | The enthalpy drop of flue gas after heat exchanging between flue gas and feed water, n = 1, 2, 3,4, 5, 6 (kJ/kg coal) |
| $\widetilde{m}_{ms}$ | The mass of the main steam produced per kg of coal (kg/kg coal) |
| $q_j$ | The specific enthalpy drop of extraction steam (kJ/kg) |

* Corresponding authors at: Institute of Engineering Thermophysics, Chinese Academy of Sciences, Beijing 100190, China (Y. Hao); School of Engineering Science, University of Science and Technology of China, Hefei 230026, China (M-B Hu).
*E-mail addresses:* haoyong@iet.cn (Y. Hao); humaobin@ustc.edu.cn (M-B Hu)

https://doi.org/10.1016/j.enconman.2019.112026
Received 20 June 2019; Received in revised form 3 September 2019; Accepted 4 September 2019
Available online xxx
0196-8904/

| | |
|---|---|
| $\tau_j$ | The specific enthalpy change of feed water (kJ/kg) |
| $\gamma_j$ | The specific enthalpy drop of drain water (kJ/kg) |
| $\alpha_i$ | The ratio of the $i^{th}$ stage of extraction steam to the mass flow of the main steam, i = 1, 2, 3…8 (–) |
| $\alpha_{rh}$ | Reheated ratio (–) |
| $\alpha_{c4}$ | The ratio of feed water through condenser to the main steam (–) |
| $\alpha_{fw}$ | The ratio of mass flow rate of feed water to the main steam (–) |
| $\alpha_{ex}$ | The excess air ratio at the boiler (–) |
| $\eta_{col}$ | Solar collector efficiency (%) |
| $\eta_{boiler}$ | Boiler efficiency (%) |
| $\eta_{exc}$ | The ratio of the heat transferred from flue gas to feed water to the enthalpy drop of flue gas in heat exchanger (%) |
| $\eta_{SEE}$ | Solar-to-electricity efficiency (%) |

***Abbreviations***

| | |
|---|---|
| DNI | Direct normal irradiation |
| SEE | Solar-to-electricity efficiency |
| PTC | Parabolic trough collector |
| ESP | Electrostatic precipitators |
| SCR | Selective catalytic reduction |
| FGD | Flue gas desulfurization |
| SAGT | Solar-aided flue gas treatment |
| SAPG | Solar-aided power generation |
| ECO | Economizer |
| AH | Air preheater |
| Hi | Feed water heater, i = 1, 2, 3…8 |

## 1. Introduction

Coal-fired power plants generate more than 38% of world electric production in 2016, an annual output of nearly 96,064 TWh as compared with a global total of 25,082 TWh [1]. In China, coal accounted for 62.0% of the total energy consumption, with 47.5% of coal consumed nationwide being utilized for power generation [2]. With the advantages of large-scale, high-stability and low-cost, this form of power generation will continue developing for a long time. However, highly polluting flue gas could restrict its development because it might bring negative effects to human body and our environment, including fine particle matter (like PM2.5), acid rain, ozone depletion and photochemical smog [3–5]. Researchers thereby developed several methods to remove the harmful compositions away from flue gas [6]. For particle matter, several particulate control technologies have been proposed, such as mechanical collectors, fabric filters (baghouse) and electrostatic precipitators (ESP) [7,8]. As for mercury emissions, technologies including sorbent injection and particulate collection systems are proposed [9]. Flue gas desulfurization (FGD) has been widely utilized to decrease $SO_2$ in Japan and America [10], such as wet lime stone FGD [11]. In addition, there are several $NO_x$ control technologies including low $NO_x$ burner, selective catalytic reduction (SCR), selective non-catalytic reduction (SNCR) and fuel reburning [12].

The above control technologies still have limitations. As the temperature of flue gas continues decreasing along the way, devices for removing fly ash, $NO_x$, $SO_x$ and other pollutants are generally installed in a certain order. For instance, SCR device is installed in front of most devices, followed by the FGD device and then the ESP device. This kind of sequence might bring trouble to the SCR device due to the fact that the existing of $SO_2$ and fly ash will deactivate the catalyst inside the device.

The SCR process utilizes catalysts to facilitate the reaction between $NO_x$ and reducing agent such as ammonia at around 300–400 °C [13]. In traditional flue gas treatment, SCR device is generally placed between economizer and air preheater for obtaining sufficiently high operation temperature. However, in a high-dust configuration, both fly ash and $SO_2$ might damage the catalysts. In a low-dust installation, a costly hot-side ESP and a flue gas reheating system are needed for the sake of optimum operation condition [9]. Moreover, by-products such as ammonium sulfate ($(NH_4)_2SO_4$) might lead to the corrosion of downstream equipments and pore plugging of catalysts [14]. There are also fewer kinds of catalysts able to be chosen because they need properties of high sulfur resistance, good anti-corrosion and high mechanical strength.

Although appropriate temperature can be easily obtained inside boilers, unfavorable factors such as sulfur poisoning [15], ash erosion and pore plugging [9] still bring troubles to the design of flue gas treatment devices inside boilers. Flue gas treatment outside boilers thereby might be a solution. Considering that the temperature of flue gas outside boilers is too low for flue gas treatments, heat source is urgently needed. Wu et al. [16] showed a tail-end denitration system, where $NO_x$ control device is placed downstream of the wet FGD and ESP units to protect catalysts from $SO_2$ and dust, but it is much more expensive than high-dust or even low-dust configuration due to the high device cost and operation cost.

As a free, renewable and environmental-friendly energy source, solar energy is attracting more and more attention [17,18]. Han et al. once proposed several methods of integrating solar energy with coal-fired power plants [19]. The methods enhance the efficiency of power generation and the effectiveness of NO removal. However, those methods are still dependent on boilers and are not able to protect the catalysts from unfavorable factors inside boilers. Thus, we proposed an advanced concept where solar energy is utilized to heat flue gas outside boilers through a parabolic trough collector (PTC) solar field and then the heat is recovered from flue gas. Flue gas outside the boiler could be heated up to a required temperature in a range from 100 to 550 °C through a PTC solar field. Thereby the sequence of flue gas treatments could be adjusted and improved depending on their operation temperatures.

One main challenge remains, that is to recover the heat from flue gas. It might be a good choice to utilize flue gas to heat the feed water for enhancing the power generation of power plants. Because of the low-intensity of solar energy and the high-cost for solar thermal power systems, combining solar energy with power plants is a desired way. In the early works of Zoschak and Wu [20], seven heat absorbing methods of integrating solar energy into a 800 MW power plant were studied. Among different methods of integrating solar energy, feed water pre-heating has been proven to be a valuable solution with comprehensive consideration of capital costs, design and operation aspects [21]. Hu et al. [22] proposed an improved idea of solar-aided power generation (SAPG) that can solve the problems of solar-only power systems. Furthermore, they proposed three strategies to control four configuration of solar preheaters [23], and investigated the impact of the operation of non-displaced feed water heaters for SAPG [24]. Yang et al. [25] also proposed that SAPG is an efficient way to utilize solar thermal energy with medium-or-low temperature, which can generate the relatively stable electricity though the solar radiation fluctuates. On the economic side, Suresh et al. analyzed the 4-E (energy, exergy, environment and economic) of SAPG plants [26]. The results revealed that utilizing solar thermal energy to substitute the feed water heaters of coal-fired power plants shows the economic benefits. Furthermore, Zhai et al. also proposed that SAPG system would be more profitable than coal-fired power system through the way of life cycle assessment [27]. For

solar energy storage, Wu et al. analyzed a 600 MW SAPG power plant integrated with a thermal energy storage (TES) part and investigated its annual economic performance [28,29]. On the whole, SAPG is one of the most efficient and economic ways to utilize solar energy for power generation which owns advantages as follows [30,31]: (a) SAPG has higher efficiencies of first law and second law of thermodynamic than coal-fired power plant and stand-alone solar power plant; (b) SAPG can be easily and flexibly combined with existing power plants with less or no risk; (c) SAPG can be adopted as a transition from conventional energy to renewable energy.

Given the potential advantages of coupling solar-aided flue gas treatment (SAGT) and solar-aided power generation (SAPG) with coal-fired power plants, it is possible to realize simultaneous environmental protection and energy conservation through solar energy. An improved flue gas treatment sequence might be established to protect catalysts and devices from damage. In addition, there might be more options for the way flue gas is treated through this concept. Synergistic effects might be achieved between SAGT and SAPG, which are described as follows: (a) flue gas treatment outside boilers enabled by a PTC solar field; (b) arbitrary operation temperatures of approximately 100–550 °C could be obtained; (c) efficient feed water preheating enabled by high temperature flue gas. A 600 MW coal-fired power plant system coupled with SAGT and SAPG was analyzed as a case study. Analysis mainly focused on denitration technology and feed water preheating system. Chemical kinetics model and thermodynamics model were established and validated. The results show that coupling SAGT and SAPG has relatively good performances both on stability and solar-to-electricity efficiency.

## 2. Concept description

### 2.1. Solar-aided flue gas treatment (SAGT)

Air preheater and its upstream devices are defined as the boiler in this paper. Here, different improved flue gas treatment sequences are given. Fig. 1 shows the schematic diagrams of four different systems, which are mainly divided into two types, denitration inside boilers and denitration outside boilers. Since particulate control devices such as ESP have already removed the dust upstream of denitration devices, catalysts are not affected by particle matter or fly ash, as shown in Fig. 1(a). However, sulfur poisoning might be another unfavorable factor for catalytic reaction [15]. SCR devices installed between economizer (ECO) and air heater (AH) are exposed to $SO_2$ directly where deactivation, corrosion and plugging might affect the performance of catalysts [14]. Considering this problem and the costly hot-side ESP devices, tail-end denitration system, in which the denitration device is installed downstream of the FGD device, is proposed as a solution which could avoid negative effects of both fly ash and $SO_2$, as shown in Fig. 1(b). Although tail-end denitration system has superiorities in the possibility of using more active catalysts and longer catalyst life to reduce overall catalysts cost, it is still too expensive to put into practice due to flue gas reheating requirements and operation cost [9]. The amount of heat provided to meet the demand of denitration is so large that it seems extremely uneconomic. Given that solar energy is a free, renewable and environmental-friendly energy source, solar-aided flue gas treatment (SAGT) was proposed. As the most mature in technical and commercial aspects among all solar thermal technologies, PTC solar field is utilized here to replace the heater of the tail-end denitration system [32]. Fig. 1(c) shows a solar-aided tail-end denitration system and Fig. 1(d) shows another solar-aided tail-end denitration system where high temperature flue gas heats the feed water to enhance the power generation of power plants rather than heats the low temperature flue gas.

Flue gas in PTC could be heated up to a required temperature in the range from 100 to 550 °C depending on the optimum operation temperature of denitration. Eck et al. [33] proposed that PTC receivers could be able to stand a pressure of 150 bars and pressure vibrations are also allowed. The pressure of flue gas is far less than 150 bars, so it is certainly within the safe range. Besides, the coatings could stand a high temperature of up to 550 °C. Yılmaz et al. [34] also reported that the working temperature of PTC can reach up to 550 °C or even higher. Since the optimum operation temperature of SCR and NO decomposition is around 300–400 °C [9] and 400–550 °C [35] respectively, PTC solar field completely meets the requirements.

### 2.2. NO decomposition

In traditional flue gas treatment, $NO_x$ control device is generally placed between economizer and air preheater, namely, upstream of ESP and FGD for obtaining sufficiently high operation temperature. However, fly ash and $SO_2$ might damage the catalysts. There are also fewer kinds of catalysts able to be chosen because they need properties of high sulfur resistance, good anti-corrosion and high mechanical strength.

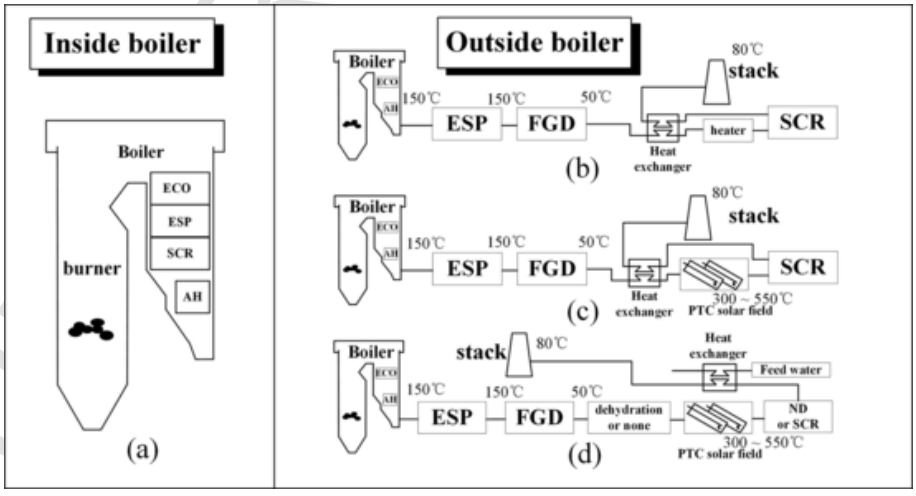


**Fig. 1.** Illustrations of different systems including: (a) a low-dust system with SCR inside boilers; (b) a tail-end denitration system with SCR outside boilers; (c) a solar-aided tail-end denitration system with SCR outside boilers, together with a heat recovery device; (d) a solar-aided tail-end denitration system with SCR or NO decomposition (ND) outside boilers, together with a feed water heating device.

The concept proposed here can not only suit the conventional $NO_x$ control technologies such as SCR, but also help to make it possible for NO decomposition. The corresponding system is shown as Fig. 1(d). Here, the denitration device is placed downstream of ESP and FGD devices, which helps to extend the life of the catalysts and improve their performances. SCR needs reducing agents such as carbon oxide (CO), hydrogen ($H_2$), ammonia ($NH_3$) and urea. These reducing agents have a high cost and might cause secondary pollutants [36]. Therefore, direct decomposition of NO ($2NO \rightarrow N_2 + O_2$) has been regarded as the most desirable method for $NO_x$ removal. Here, we used this technology to control $NO_x$.

NO molecules are thermodynamically unstable which is favorable for NO decomposition because the enthalpy of formation of NO is large and positive, $\Delta H^0_{f\,(298K)} = 90.2\,kJ/mol$. Nevertheless, its activation energy is too high for homogeneous decomposition of NO, at about 335 kJ/mol, since that the N-O bond is difficult to break, and its interatomic distance is between the double-bond distance and the triple-bond distance [37]. Thus, catalyst plays an important role in decreasing the activation energy of the reaction. Among various catalysts, copper ion-exchanged MFI zeolite (Cu-ZSM-5) reported by Iwamoto et al. [38,39] is the most active catalyst for NO decomposition even at relatively low temperature around 400–550 °C [35]. It shows high activity in the presence of $O_2$ and would almost not be affected by $CO_2$ when compared with other catalysts such as perovskite oxide catalyst [40,41].

### 2.3. Coupling solar-aided flue gas treatment (SAGT) and solar-aided power generation (SAPG)

Fig. 2 shows a schematic diagram of the advanced concept, combining SAGT with SAPG, which corresponds to Fig. 1(d). It depicts more details including flue gas emission path, boiler structure, feed water preheating system and the combination between devices and the PTC solar field.

As shown in Fig. 2(a) and (b), high temperature flue gas is produced in burner and then it passes through super-heaters, re-heaters, ECO, AH, ESP in the order before out of boilers. Since $SO_x$ and $NO_x$ derived from the exhaust have serious pollution, further treatments should be done to flue gas. As a most common technology of $SO_x$-removal worldwide, wet limestone FGD is used in SAGT with its high removal rate of over 95% [42]. For $NO_x$-removal, SCR process needs an optimum operation temperature of approximately 300–400 °C [9] which can be easily obtained through PTC solar field. In addition, it has no requirement on low humidity of flue gas, so there is no need to dehumidify or dehydrate. Flue gas could be heated by PTC solar field and sent to SCR device right after FGD device. NO decomposition requires an optimum operation temperature of around 400–550 °C [35] and the temperature can also be obtained by PTC solar field. However, it has a high requirement on low humidity of flue gas. As a result, flue gas needs dehumidification and dehydration devices after FGD device.

Almost all coal-fired power plants are working in the Regenerative Rankine Cycle. Using steam extracted from turbine to preheat boiler feed water is a usual way to increase the overall thermal efficiency of the power plant [43,44]. In a SAPG system, solar energy is absorbed into oil or water. Here the situation is different. As shown in Fig. 2(b), solar energy is absorbed by flue gas and then the heat is transferred from high temperature flue gas to feed water. SAPG is thereby realized by replacing part or all extraction steam with the flue gas through heat exchangers.

Solar energy is a free, renewable and environmental-friendly energy source, however with an obvious shortcoming in the demand of stable and continuous supply. Designing a thermal energy storage (TES) device and an auxiliary heating boiler (AHB) could solve the unstable problem of solar energy. The devices would be installed between solar field and denitration device to stabilize the temperature of flue gas, which can be seen in Fig. 2(a). If the temperature of flue gas is higher than the required temperature, molten salt from the cold salt tank would absorb the heat from high temperature flue gas through the exchanger. Then the molten salt would be stored in a hot salt tank. If the temperature of flue gas is lower than the required temperature, molten salt from the hot salt tank could be utilized to heat the flue gas. Then it would be stored in a cold salt tank. In addition, auxiliary heating boiler is utilized to provide additional required heat when the weather is cloudy or rainy continuously.

## 3. Modeling

As shown in Fig. 3, two calculation paths couple with each other. Both of them start from "1kg coal" because the amount of flue gas and the main stream are both dependent on the mass of coal consumption. The following statements are based on assumption of burning 1 kg of coal.

The first path is about various treatments of flue gas including pollutants removal and flue gas heating. In Section 3.1, the mole fractions and the amounts of substance of $NO_x$, $CO_2$, $O_2$ and $N_2$ after gas pretreatments are shown. The mole fractions provide basic data for the chemical kinetics calculations in Section 3.2. The amounts of substance are utilized for the calculations of solar field in Section 3.3.1. The collector aperture area of solar field depends on the heat demand

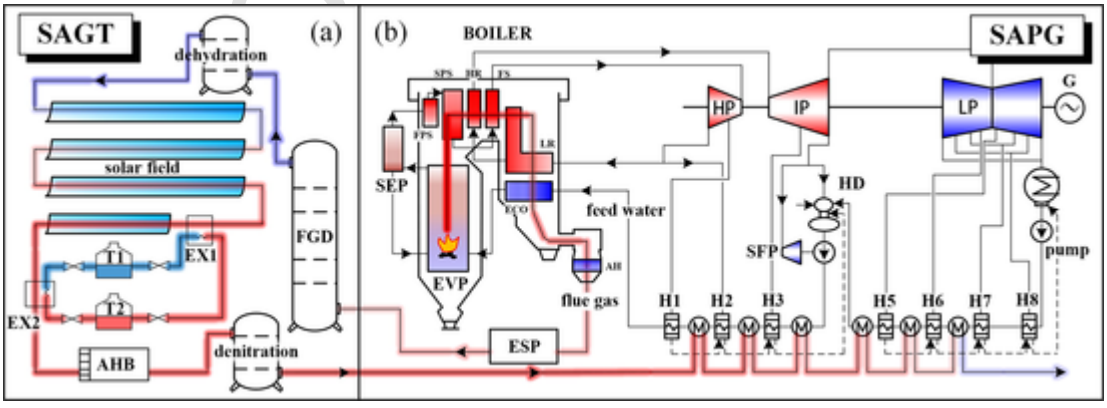


**Fig. 2.** Schematic diagram of the concept consisting of: (a) solar-aided flue gas treatment (SAGT) and (b) solar-aided power generation (SAPG). EX: exchanger for Thermal flue gas/Molten salt; T1: cold salt tank; T2: hot salt tank; AHB: auxiliary heating boiler; SEP: steam separator; FPS: first platen super-heater; SPS: second platen super-heater; FS: final super-heater; LR: low-temperature re-heater; HR: high-temperature re-heater; EVP: evaporator; HP: high-pressure turbine; IP: intermediate-pressure turbine; LP: low-pressure turbine; SFP: steam feed pump; HD: high-pressure deaerator; G: generator.

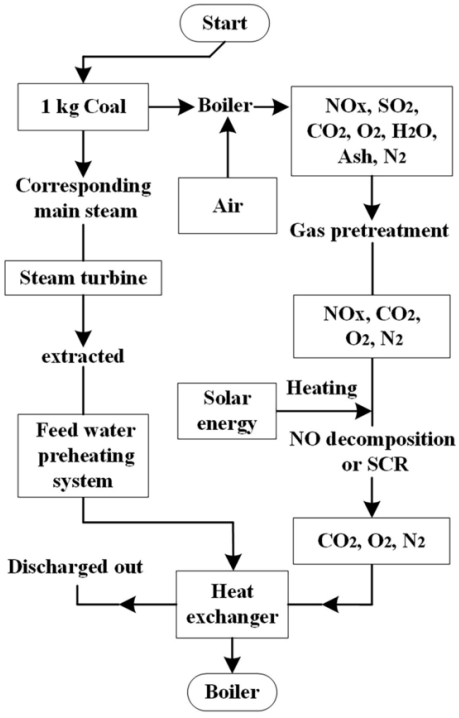


**Fig. 3.** Flow chart of solar-aided flue gas treatment (SAGT) and solar-aided power generation (SAPG).

of flue gas. The gas pretreatments include removal of dust, $SO_2$ and water vapor.

The second path is about feed water preheating system. The amount of the main steam depends on the acquired heat from fuel. The amount of feed water and extraction steam are related to the main steam, whose calculations are shown in Sections 3.3.2 and 3.3.4. Finally, two paths are coupled through heat exchangers for the thermodynamic calculations.

### 3.1. Combustion calculation of fuel

Calculations for combustion products are based on the proximate and ultimate analysis of raw anthracite coal [45]. The constituents and percentage contents of the as received basis are calculated and listed in Table 1. The products mainly include $CO_2$, $H_2O$, $O_2$, $N_2$, $NO_x$ (approximately 90%) [4] and $SO_2$. The details of calculation are presented in the Appendix A. And calculation results of the percentage contents are listed as Table 2 which shows the molar ratio of the components in flue gas.

**Table 1**
Components and relative contents of as received basis of the raw anthracite.

| Items | Data (%) |
|---|---|
| Moisture | 3.37 |
| Ash | 8.47 |
| Carbon | 81.48 |
| Hydrogen | 3.11 |
| Oxygen | 1.70 |
| Nitrogen | 1.17 |
| Sulfur | 0.70 |
| Total | 100.0 |

**Table 2**
Molar ratio of the components in flue gas.

| Item | Unit | Molar ratio |
|---|---|---|
| $NO_x$ | ppm | 551.488 |
| $CO_2$ | % | 16.005 |
| $O_2$ | % | 3.560 |
| $N_2$ | % | 80.426 |
| Total | % | 100 |

### 3.2. Chemical kinetics model of NO decomposition

In this study, we chose NO decomposition technology as the denitration method in SAGT, since NO decomposition technology has been considered as one of the most desirable approaches to control $NO_x$ [40]. It is necessary to study its chemical kinetics to show the possibility and performances. Because volume fraction of NO is too small to affect the temperature of flue gas, reaction heat of NO decomposition can be ignored. One of the key results that we desire is the conversion rate of NO decomposition. The reaction is given as $2NO \rightarrow N_2 + O_2$. For NO decomposition reaction, the mechanism and reaction kinetics here are based on Ref. [46]. The reaction rate of NO decomposition ($r_{NO}$) is relevant to the concentrations of NO ($c_{NO}$) and $O_2$ ($c_{O2}$). The concentrations of NO and $O_2$ are dependent on the partial pressure of NO and $O_2$. The decomposition rate gets faster with higher concentration of NO, while presence of $O_2$ would inhibit the reaction. Conversion rate is calculated as follows:

$$\beta_{cov} = \left| \frac{c_{NO,\,0} - c_{NO}}{c_{NO,\,0}} \right| \times 100\% \tag{1}$$

where $c_{NO,\,0}$ is the initial concentration of NO, mol/m$^3$, expressed as:

$$c_{NO,0} = \frac{n_{NO,0}}{V} = \frac{\varphi_{NO,0} \cdot P_{reac}}{R \cdot T_{reac}} \tag{2}$$

where $c_{NO,\,0}$ is the initial concentration of NO per unit volume, mol/m$^3$; $V$ is a unit volume, here is assigned as 1 m$^3$; $\varphi_{NO,\,0}$ is the initial volume fraction of NO; $P_{reac}$ is the pressure of flue gas in the reactor, Pa; $R$ represents perfect gas constant, 8.314 J/(mol·K); $T_{reac}$ is the temperature of flue gas in the reactor, K.

The equation of concentration of NO ($c_{NO}$) is derived from Eqs. (3) and (4) and expressed as Eq. (5). Its reaction rate ($r_{NO}$) is expressed as Eq. (4) according to Ref. [46]. They are as follows:

$$dc_{NO} = -r_{NO} \cdot d\tau \tag{3}$$

$$r_{NO} = \frac{k_{app} \cdot c_{NO}^2}{1 + K_\alpha \cdot c_{O_2}^{1/2}} \tag{4}$$

$$c_{NO}(\tau) = \left( \frac{1}{c_{NO,\,0}} + \frac{k_{app} \cdot \tau}{1 + K_\alpha \cdot c_{O_2}^{1/2}} \right)^{-1} \tag{5}$$

where $\tau$ represents the residence time or reaction time, s; $c_{O_2}$ is the concentration of $O_2$, mol/m$^3$; the apparent rate constants ($k_{app}$) and equilibrium constant ($K_\alpha$) for $O_2$ adsorption are of Arrhenius form and are given as Eqs. (6) and (7), respectively.

$$k_{app} = A_{app} \cdot e^{-E_{app}/(R \cdot T_{reac})} \tag{6}$$

$$K_\alpha = A_\alpha \cdot e^{-\Delta H_\alpha/(R \cdot T_{reac})} \tag{7}$$

where $A_{app}$ and $A_\alpha$ are preexponential factors; $E_{app}$ represents apparent activation energy, kJ/mol; $\Delta H_\alpha$ is enthalpy change of adsorption, kJ/mol.

### 3.3. Thermodynamic model of SAPG

The overall thermodynamic system diagram is shown as Fig. 4. The main variables of solar field and boiler are marked in the figure, and the corresponding modeling is built in the following Sections 3.3.1 and 3.3.2. In addition, main variables and the modeling of feed water preheating system are given in Sections 3.3.4 and 3.3.5.

#### 3.3.1. Solar field

The logic flow chart of turbine and feed water preheating system simulation model is presented in Fig. 5, where calculation results of solar-to-electricity efficiency (SEE) is dependent on the inputs of direct normal irradiation (DNI), incidence angle and heating temperature. Since that the amount of $NO_x$ is extremely small, heat absorbed by $NO_x$ is ignored in following calculations. The enthalpy of flue gas after denitration is expressed as:

$$\widetilde{h}_{\mathrm{fg}} = h_{\mathrm{CO_2}} \cdot \widetilde{n}_{\mathrm{CO_2}} + h_{\mathrm{O_2}} \cdot \widetilde{n}_{\mathrm{O_2}} + h_{\mathrm{N_2}} \cdot \widetilde{n}_{\mathrm{N_2}} \tag{8}$$

where $\widetilde{h}_{\mathrm{fg}}$ is the enthalpy of flue gas produced by burning 1 kg coal, which mainly consists of nitrogen ($N_2$), oxygen ($O_2$) and carbon dioxide ($CO_2$), kJ/kg coal; $h_{CO2}$, $h_{O2}$, $h_{N2}$ represent the specific molar enthalpy of $CO_2$, $O_2$ and $N_2$, respectively, kJ/mol, which depends on the temperature of flue gas (data from NIST [47]); $\widetilde{n}_{\mathrm{CO_2}}$, $\widetilde{n}_{\mathrm{O_2}}$, $\widetilde{n}_{\mathrm{N_2}}$ represent the amount of substance of $CO_2$, $O_2$ and $N_2$ produced by 1 kg coal, respectively, mol/kg coal.

A PTC solar field is used to heat flue gas. The thermal energy obtained by flue gas depends on the absorbed solar energy. The thermal energy absorbed by flue gas $\dot{Q}_{\mathrm{abs}}$ can be expressed by:

$$\dot{Q}_{abs} = I \cdot A_{sf} \cdot \eta_{col} = \left(\widetilde{h}_{fg,osf} - \widetilde{h}_{fg,isf}\right) \cdot \dot{m}_{coal} \times 10^3 \tag{9}$$

where $I$ represents the DNI of sun light that is projected on the collector aperture area, W/m$^2$; $A_{\mathrm{sf}}$ is the collector aperture area of solar field, m$^2$; $\eta_{\mathrm{col}}$ is the solar collector efficiency, %, the calculation details of which are shown in Appendix B; $\widetilde{h}_{\mathrm{fg,\ osf}}$ is the enthalpy of flue gas in the outlet of solar field, kJ/kg coal; $\widetilde{h}_{\mathrm{fg,\ isf}}$ is the enthalpy of flue gas in the inlet of solar field, kJ/kg coal; $\dot{m}_{\mathrm{coal}}$ is the consumption rate of coal, kg/s.

#### 3.3.2. Boiler

According to the concept of SAGT & SAPG, after being produced in boiler and then heated by PTC solar field, the flue gas transfers the heat to feed water, which might replace a part of the extraction steam, as shown in Fig. 4. The heat balance of the boiler depends on the mass flow rates of the main steam and reheat steam as well as the enthalpy differences of water between outlet and inlet of boiler. The model is established based on the thermodynamic calculation method of the former Soviet Union in 1973 and modified in China in 1998 [48]. The heat balance in the boiler is given as follows:

$$\begin{aligned}\dot{Q}_{\mathrm{b}} &= \dot{m}_{\mathrm{ms}}\left(h_{\mathrm{ms}} - h_{\mathrm{fw}}\right) + \dot{m}_{\mathrm{rh}}\left(h_{\mathrm{rho}} - h_{\mathrm{rhi}}\right) \\ &= \dot{m}_{\mathrm{coal}} \cdot \widetilde{Q}_{\mathrm{f}} \cdot \eta_{\mathrm{boiler}}\end{aligned} \tag{10}$$

where $\dot{Q}_{\mathrm{b}}$ is the total heat absorbed by water in the boiler; $\dot{m}_{\mathrm{ms}}$ and $\dot{m}_{\mathrm{rh}}$ are the mass flow rates of the main steam and reheat steam, kg/s, respectively; $h_{\mathrm{ms}}$ is the specific enthalpy of the main steam and $h_{\mathrm{fw}}$ is the specific enthalpy of feed water, kJ/kg; $h_{\mathrm{rho}}$ and $h_{\mathrm{rhi}}$ are the specific enthalpies of reheat steam in the outlet and inlet of the boiler, kJ/kg, respectively; $\widetilde{Q}_{\mathrm{f}}$ is the low heating value of the raw anthracite mentioned in Section 3.1, and the value is 30700 kJ/kg coal [45]; $\eta_{\mathrm{boiler}}$ represents the boiler efficiency and is assigned as 92.5% for simplification of the calculations [49].

#### 3.3.3. Feed water preheating system

The calculation model of the heaters is built as Eqs. (11)–(20). In order to ensure that the temperature of the flue gas can reach approximately 80 °C before entering the stack, as shown in Fig. 1, flue gas would not transfer the heat to feed water after the 6th heat exchanger as described in Eqs. (17) and (18). The calculations are expressed as:

$$\frac{\Delta\widetilde{h}_{\mathrm{fg,\ 1}} \cdot \eta_{exc}}{\widetilde{m}_{\mathrm{ms}}} + \alpha_1 \cdot q_1 = \alpha_{\mathrm{fw}} \cdot \tau_1 \tag{11}$$

$$\frac{\Delta\widetilde{h}_{\mathrm{fg,\ 2}} \cdot \eta_{exc}}{\widetilde{m}_{\mathrm{ms}}} + \alpha_2 \cdot q_2 + \alpha_1 \cdot \gamma_2 = \alpha_{\mathrm{fw}} \cdot \tau_2 \tag{12}$$

$$\frac{\Delta\widetilde{h}_{\mathrm{fg,\ 3}} \cdot \eta_{exc}}{\widetilde{m}_{\mathrm{ms}}} + \alpha_3 \cdot q_3 + \left(\alpha_1 + \alpha_2\right)\gamma_3 = \alpha_{\mathrm{fw}} \cdot \tau_3 \tag{13}$$

$$\frac{\Delta\widetilde{h}_{\mathrm{fg,\ 4}} \cdot \eta_{exc}}{\widetilde{m}_{\mathrm{ms}}} + \alpha_4 \cdot q_4 + \left(\alpha_1 + \alpha_2 + \alpha_3\right)\gamma_4 = \alpha_{\mathrm{fw}} \cdot \tau_4 \tag{14}$$

$$\frac{\Delta\widetilde{h}_{\mathrm{fg,\ 5}} \cdot \eta_{exc}}{\widetilde{m}_{\mathrm{ms}}} + \alpha_5 \cdot q_5 = \alpha_{\mathrm{c4}} \cdot \tau_5 \tag{15}$$

$$\frac{\Delta\widetilde{h}_{\mathrm{fg,\ 6}} \cdot \eta_{exc}}{\widetilde{m}_{\mathrm{ms}}} + \alpha_6 \cdot q_6 + \alpha_5 \cdot \gamma_5 = \alpha_{\mathrm{c4}} \cdot \tau_6 \tag{16}$$

$$\alpha_7 \cdot q_7 + \left(\alpha_5 + \alpha_6\right)\gamma_7 = \alpha_{\mathrm{c4}} \cdot \tau_7 \tag{17}$$

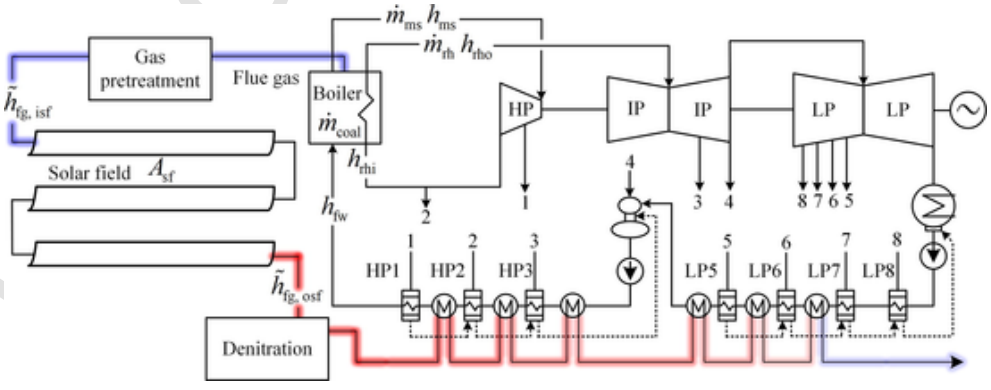


**Fig. 4.** Overall thermodynamic system diagram of the 600 MW coal-fired power plant coupled with SAGT and SAPG.

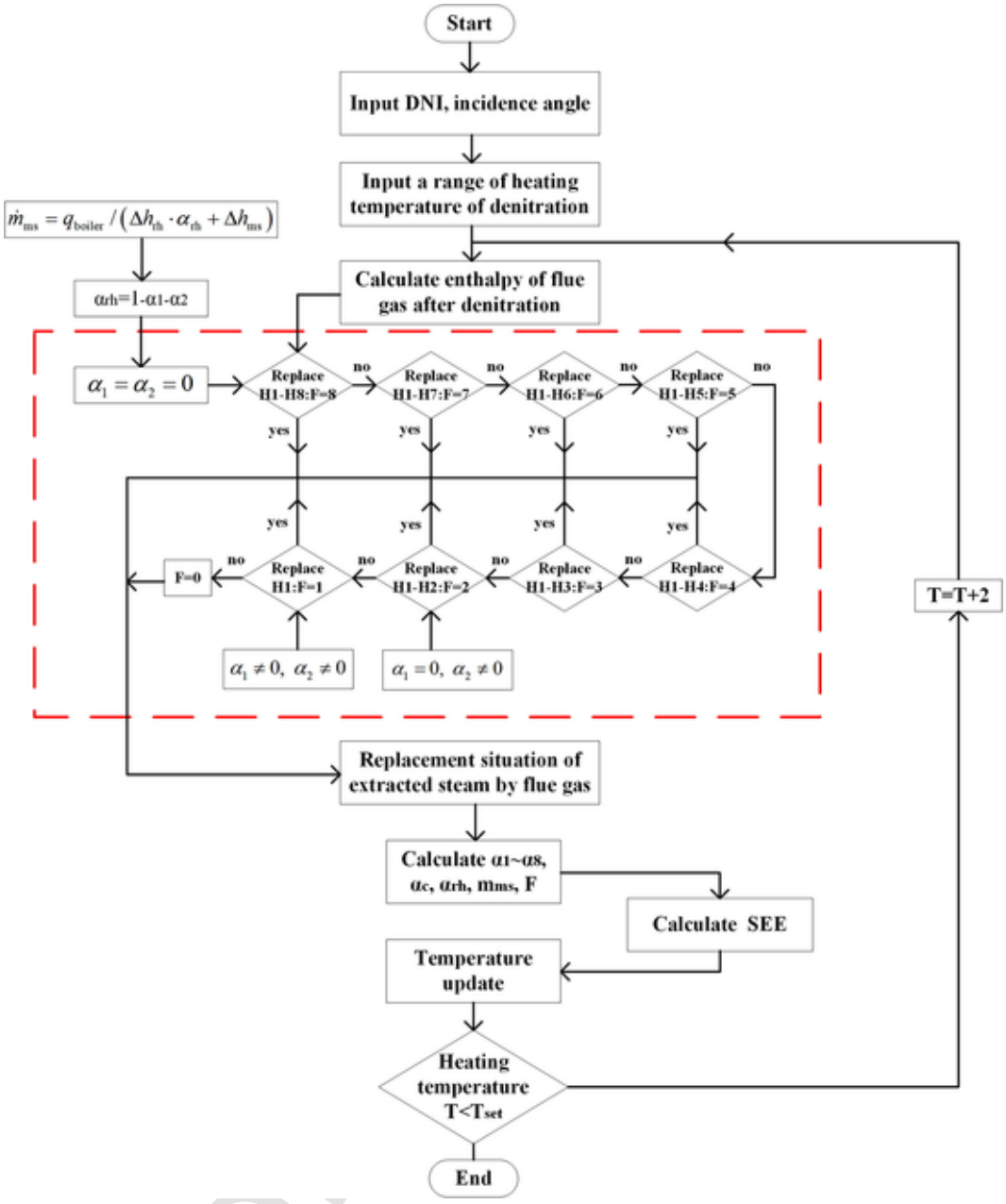


**Fig. 5.** Logic flow chart of turbine and feed water preheating system simulation model.

$$\alpha_8 \cdot q_8 + (\alpha_5 + \alpha_6 + \alpha_7)\,\gamma_8 = \alpha_{c4} \cdot \tau_8 \tag{18}$$

$$\alpha_{c4} = \alpha_{fw} - (\alpha_1 + \alpha_2 + \alpha_3 + \alpha_4) \tag{19}$$

$$\alpha_{rh} = 1 - \alpha_1 - \alpha_2 \tag{20}$$

where $\Delta\widetilde{h}_{fg,\,n}$ is the enthalpy drop of flue gas produced by 1 kg coal before and after heat exchanging between flue gas and feed water in the $n^{th}$ heat exchanger (n = 1, 2, 3, 4, 5, 6) as shown in Fig. 4, kJ/kg coal; $\eta_{exc}$ represents the ratio of the heat transferred from flue gas to feed water to the enthalpy drop of flue gas in heat exchanger, which is given in Appendix C, %. $\widetilde{m}_{ms}$ is the mass of the main steam, which can also be expressed as the ratio of mass flow rate of the main steam to the consumption rate of coal ($\dot{m}_{ms}/\dot{m}_{coal}$), kg/kg coal; $\alpha_i$ is the ratio of extraction steam to mass flow rate of the main steam in the $i^{th}$ stage extraction (i = 1, 2, 3, 4, 5, 6, 7, 8), which is also called extraction coefficient; $\alpha_{c4}$ is the ratio of feed water in the low pressure side to mass flow rate of the main steam; $\alpha_{rh}$ is the ratio of reheat water to mass flow rate of the main steam ($\dot{m}_{rh}/\dot{m}_{ms}$).

The specific enthalpy drop of the extraction steam ($q_j$), the specific enthalpy change of feed water ($\tau_j$), the specific enthalpy drop of drain water ($\gamma_j$) in the $j^{th}$ heater and $\Delta\widetilde{h}_{fg,\,n}$ is discussed as follows:

$$q_j = \begin{cases} h_j - h'_j & (j = 1, 2, 3, 5, 6, 7, 8) \\ h_j - h_{wj+1} & (j = 4) \end{cases} \tag{21}$$

$$\tau_j = h_{wj} - h_{wj+1}\ (j = 1, 2, 3, 4, 5, 6, 7, 8) \tag{22}$$

$$\gamma_j = \begin{cases} h'_{j-1} - h'_j & (j = 1, 2, 3, 5, 6, 7, 8) \\ h'_{j-1} - h_{wj+1} & (j = 4) \end{cases} \tag{23}$$

$$\Delta\widetilde{h}_{fg,\,n} = \widetilde{h}_{fg,\,n-1} - \widetilde{h}_{fg,\,n}\ (n = 1, 2, 3, 4, 5, 6) \tag{24}$$

where $h_j$ represents the specific enthalpy of extraction steam in the feed water heater; $h_{wj}$ is the specific enthalpy of feed water in the outlet of the $j^{th}$ heater; $h_j'$ means the specific enthalpy of drain water in the $j^{th}$ heater.

According to Eqs. (11)–(24), matrix energy balance equation can be expressed as:

$$\begin{bmatrix} q_1 & & & & & & & \\ \gamma_2 & q_2 & & & & & & \\ \gamma_3 & \gamma_3 & q_3 & & & & & \\ \gamma_4 & \gamma_4 & \gamma_4 & q_4 & & & & \\ \tau_5 & \tau_5 & \tau_5 & \tau_5 & q_5 & & & \\ \tau_6 & \tau_6 & \tau_6 & \tau_6 & \gamma_6 & q_6 & & \\ \tau_7 & \tau_7 & \tau_7 & \tau_7 & \gamma_7 & \gamma_7 & q_7 & \\ \tau_8 & \tau_8 & \tau_8 & \tau_8 & \gamma_8 & \gamma_8 & \gamma_8 & q_8 \end{bmatrix} \begin{bmatrix} \alpha_1 \\ \alpha_2 \\ \alpha_3 \\ \alpha_4 \\ \alpha_5 \\ \alpha_6 \\ \alpha_7 \\ \alpha_8 \end{bmatrix} + \frac{\eta_{exc}}{\widetilde{m}_{ms}} \begin{bmatrix} \Delta\widetilde{h}_{fg,1} \\ \Delta\widetilde{h}_{fg,2} \\ \Delta\widetilde{h}_{fg,3} \\ \Delta\widetilde{h}_{fg,4} \\ \Delta\widetilde{h}_{fg,5} \\ \Delta\widetilde{h}_{fg,6} \\ 0 \\ 0 \end{bmatrix} = \alpha_{fw} \begin{bmatrix} \tau_1 \\ \tau_2 \\ \tau_3 \\ \tau_4 \\ \tau_5 \\ \tau_6 \\ \tau_7 \\ \tau_8 \end{bmatrix} \tag{25}$$

*3.3.4. Signal "F"*

How to combine heat exchangers with the feed water preheating system was discussed in detail here. High temperature flue gas is utilized to replace the extraction steam from turbine, and the calculation method differs from the original situation. As shown in the red dotted box of Fig. 5, a subprogram is used to determine how many levels of feed water heaters can be replaced by heat exchangers, and a signal "F" is given to represent the number of heaters that could be replaced. Different designed flue gas temperature corresponds to different signal "F". For example, "F = 2" means there are 2 heaters replaced. Moreover, the extraction coefficients of feed water preheating system will change with different signal "F". For instance, as the signal shows "F = 3", extraction coefficients $\alpha_1 - \alpha_3$ are assigned as 0 and $\alpha_4 - \alpha_8$ might become smaller, which boosts the total power generation of power plants. After obtaining the values of extraction coefficients ($\alpha_1 - \alpha_8$), condensation coefficient ($\alpha_c$), reheat coefficient ($\alpha_{rh}$), mass of the main steam produced per kg of coal ($\widetilde{m}_{ms}$), signal "F", we can calculate the SEE of the whole system. Then designed flue gas temperature is updated to a new value, and the calculation process repeats again until heating temperature reaches the set value ($T_{set}$).

Fig. 6 shows the details of feed water preheating system coupled with flue gas heat exchangers. Feed water preheating system generally has 3 high pressure heaters, 1 deareactor and 4 low pressure heaters, while this system has 3 high pressure heater, 1 deareactor, 4 low pressure heaters and 6 heat exchangers. Eq. (25) only works at the situation of "F = 0". If signal shows "F > 0", the value of $\Delta\widetilde{h}_{fg,1} \cdot \eta_{exc}$ becomes bigger than $\alpha_{fw} \cdot \tau_1 \cdot \widetilde{m}_{ms}$ and $\alpha_1$ becomes negative, which is not allowed in practice. Thereby study on how signal works becomes an important task. Signal "F = n" should meet the following conditions:

$$\begin{cases} \dfrac{\left(\widetilde{h}_{fg,0} - \widetilde{h}_{fg,n}\right)\eta_{exc}}{\widetilde{m}_{ms}} > \alpha_{fw}\left(h_{w,1} - h_{w,n+1}\right) \\ AND \\ \dfrac{\left(\widetilde{h}_{fg,0} - \widetilde{h}_{fg,n+1}\right)\eta_{exc}}{\widetilde{m}_{ms}} < \alpha_{fw}\left(h_{w,1} - h_{w,n+2}\right) \\ (n = 0, 1, 2) \end{cases} \tag{26}$$

$$\begin{cases} \dfrac{\left(\widetilde{h}_{fg,0} - \widetilde{h}_{fg,n}\right)\eta_{exc}}{\widetilde{m}_{ms}} > \alpha_{fw}\left(h_{w,1} - h_{w,4}\right) + \alpha_{c4}\left(h_{w,4} - h_{w,n+1}\right) \\ AND \\ \dfrac{\left(\widetilde{h}_{fg,0} - \widetilde{h}_{fg,n+1}\right)\eta_{exc}}{\widetilde{m}_{ms}} < \alpha_{fw}\left(h_{w,1} - h_{w,4}\right) + \alpha_{c4}\left(h_{w,4} - h_{w,n+2}\right) \\ (n = 3, 4, 5, 6) \end{cases} \tag{27}$$

where $\widetilde{h}_{fg,0}$ represents the enthalpy of flue gas right after denitration and before heat exchanging, kJ/kg coal; $\widetilde{h}_{fg,i}$ is the enthalpy of flue gas out of the $n^{th}$ heat exchanger, kJ/kg coal, as shown in Fig. 6.

Matrix energy balance equations corresponding to different signal "F" are given as Eqs. (28)–(30), where signals "F" are assigned as 1, 2, 3, respectively. Through these equations, we can conclude the equations corresponding to "F = 4, 5, 6" by following the same rules.

(a) $F = 1, \alpha_1 = 0$

$$\begin{bmatrix} q_2 & & & & & & \\ \gamma_3 & q_3 & & & & & \\ \gamma_4 & \gamma_4 & q_4 & & & & \\ \tau_5 & \tau_5 & \tau_5 & q_5 & & & \\ \tau_6 & \tau_6 & \tau_6 & \gamma_6 & q_6 & & \\ \tau_7 & \tau_7 & \tau_7 & \gamma_7 & \gamma_7 & q_7 & \\ \tau_8 & \tau_8 & \tau_8 & \gamma_8 & \gamma_8 & \gamma_8 & q_8 \end{bmatrix} \begin{bmatrix} \alpha_2 \\ \alpha_3 \\ \alpha_4 \\ \alpha_5 \\ \alpha_6 \\ \alpha_7 \\ \alpha_8 \end{bmatrix} + \frac{\eta_{exc}}{\widetilde{m}_{ms}} \begin{bmatrix} \Delta\widetilde{h}_{fg,1} + \Delta\widetilde{h}_{fg,2} \\ \Delta\widetilde{h}_{fg,3} \\ \Delta\widetilde{h}_{fg,4} \\ \Delta\widetilde{h}_{fg,5} \\ \Delta\widetilde{h}_{fg,6} \\ 0 \\ 0 \end{bmatrix} = \alpha_{fw} \begin{bmatrix} \tau_1 + \tau_2 \\ \tau_3 \\ \tau_4 \\ \tau_5 \\ \tau_6 \\ \tau_7 \\ \tau_8 \end{bmatrix} \tag{28}$$

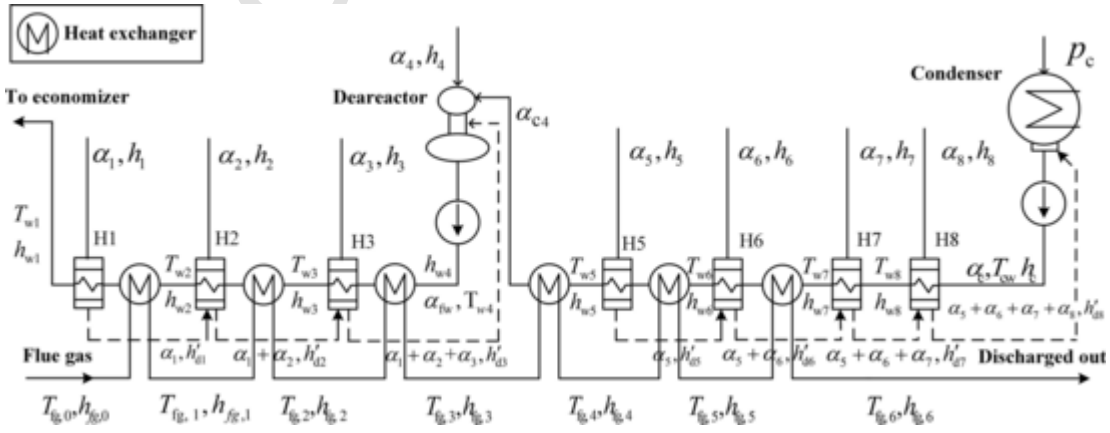


**Fig. 6.** Thermodynamic system diagram of feed water preheating coupled with a flue gas heat exchanging subsystem.

(b) $F = 2, \alpha_1 = \alpha_2 = 0$

$$\begin{bmatrix} q_3 & & & & & \\ \gamma_4 & q_4 & & & & \\ \tau_5 & \tau_5 & q_5 & & & \\ \tau_6 & \tau_6 & \gamma_6 & q_6 & & \\ \tau_7 & \tau_7 & \gamma_7 & \gamma_7 & q_7 & \\ \tau_8 & \tau_8 & \gamma_8 & \gamma_8 & \gamma_8 & q_8 \end{bmatrix} \begin{bmatrix} \alpha_3 \\ \alpha_4 \\ \alpha_5 \\ \alpha_6 \\ \alpha_7 \\ \alpha_8 \end{bmatrix} + \frac{\eta_{exc}}{\widetilde{m}_{ms}} \begin{bmatrix} \Delta\widetilde{h}_{fg,1} + \Delta\widetilde{h}_{fg,2} + \Delta\widetilde{h}_{fg,3} \\ \Delta\widetilde{h}_{fg,4} \\ \Delta\widetilde{h}_{fg,5} \\ \Delta\widetilde{h}_{fg,6} \\ 0 \\ 0 \end{bmatrix} = \alpha_{fw} \begin{bmatrix} \tau_1 + \tau_2 + \tau_3 \\ \tau_4 \\ \tau_5 \\ \tau_6 \\ \tau_7 \\ \tau_8 \end{bmatrix} \tag{29}$$

(c) $F = 3, \alpha_1 = \alpha_2 = \alpha_3 = 0$

$$\begin{bmatrix} q_4 & & & & \\ \tau_5 & q_5 & & & \\ \tau_6 & \gamma_6 & q_6 & & \\ \tau_7 & \gamma_7 & \gamma_7 & q_7 & \\ \tau_8 & \gamma_8 & \gamma_8 & \gamma_8 & q_8 \end{bmatrix} \begin{bmatrix} \alpha_4 \\ \alpha_5 \\ \alpha_6 \\ \alpha_7 \\ \alpha_8 \end{bmatrix} + \frac{\eta_{exc}}{\widetilde{m}_{ms}} \begin{bmatrix} \Delta\widetilde{h}_{fg1} + \Delta\widetilde{h}_{fg2} + \Delta\widetilde{h}_{fg3} + \Delta\widetilde{h}_{fg4} \\ \Delta\widetilde{h}_{fg5} \\ \Delta\widetilde{h}_{fg6} \\ 0 \\ 0 \end{bmatrix} = \alpha_{fw} \begin{bmatrix} \tau_1 + \tau_2 + \tau_3 + \tau_4 \\ \tau_5 \\ \tau_6 \\ \tau_7 \\ \tau_8 \end{bmatrix} \tag{30}$$

*3.3.5. Off-design condition*

In this paper, we showed both the performances of design condition and off-design condition of this concept. In the situation of off-design condition, the main and reheat steam will inevitably be affected. Thus, variable operation conditions should be taken into account. Here, the improved Flugel formula is utilized to simplify the calculation, which is shown as [50]:

$$\frac{\dot{m}'_i}{\dot{m}_i} = \sqrt{\frac{p'^2_i - p'^2_{i+1}}{p^2_i - p^2_{i+1}}} \tag{31}$$

where $\dot{m}'_i$ and $\dot{m}_i$ are the steam mass flow rate of the $i^{th}$ stage of the turbine under off-design condition and original design condition, respectively, kg/s; $p'_i$ and $p'_{i+1}$ are pressure of the $i^{th}$ and $(i+1)^{th}$ stage in turbine under off-design condition, MPa; $p_i$ and $p_{i+1}$ are pressure of the $i^{th}$ and $(i+1)^{th}$ stage in turbine under original design condition, MPa.

*3.4. Evaluation criteria of solar-aided power generation (SAPG)*

For design conditions, steam parameters of the first and second stage are set to fixed values. The steam pressure and temperature in the inlet and outlet of the boiler reheater are also given fixed values, where the fixed values are the same as the reference power plant [49]. If these values are changed, the design of the economizer and reheater in the boiler will be affected, which is unfavorable for the independence of SAPG from boilers. We calculated the solar-to-electricity efficiency (SEE) based on the power boost mode in the study. SEE is the ratio of electric power generated by solar thermal energy to the solar energy projected on the collector aperture area, shown as:

$$\eta_{SEE} = \frac{\dot{E}_{solar}}{10^{-6} \cdot I \cdot A_{sf}} = \frac{\dot{E}_{SAPG} - 10^{-3} \cdot \dot{Q}_b \cdot \eta_{ref}}{10^{-6} \cdot I \cdot A_{sf}} \times 100\% \tag{32}$$

where $\dot{E}_{solar}$ is the electric power generated by solar thermal energy, MW; $\dot{E}_{SAPG}$ represents the overall electric power generated by solar-aided coal-fired power plant, MW; $\eta_{ref}$ is the cycle efficiency of the reference power plant; $I$ and $A_{sf}$ have been expressed as Eq. (9).

## 4. Results and discussions

In order to protect catalysts from unfavorable factors such as sulfur poisoning, corrosion and blockage, an improved flue gas treatment sequence is proposed. Utilization of solar energy realizes the flue gas treatment outside boilers, which makes it possible for NO decomposition technology to put into practice. Furthermore, high temperature flue gas could be utilized to heat the feed water for enhancing the power generation of power plants. To analyze the performances of the above calculation model, a 600 MW coal-fired power plant coupled with SAGT and SAPG is investigated as a case study. The simplified thermodynamic system diagrams have been presented in Figs. 4 and 6. Validations of both chemical kinetics model and SAPG model are also presented in the following parts.

### 4.1. Validation

#### 4.1.1. Chemical kinetics model

Parameters such as $A_{app}$, $A_\alpha$, $E_{app}$ and $\Delta H_\alpha$ can be obtained from the experimental results of Ref. [46]. Those data give values of $5.9987 \times 10^{-3}$ for $A_{app}$, $2.2834 \times 10^{-5}$ for $A_\alpha$, −45.98 kJ/mol for $E_{app}$ and −75.24 kJ/mol for $\Delta H_\alpha$, respectively. Experimental results from the reference are compared with simulation results as shown in Fig. 7, with the conditions of 1 kPa NO/He at 673 K and 1.013 bar. The relative errors between simulation results and the literature are below 7%, which indicates that the kinetic model is acceptable. On the whole, the relative error decreases as the residence time increases. The reason

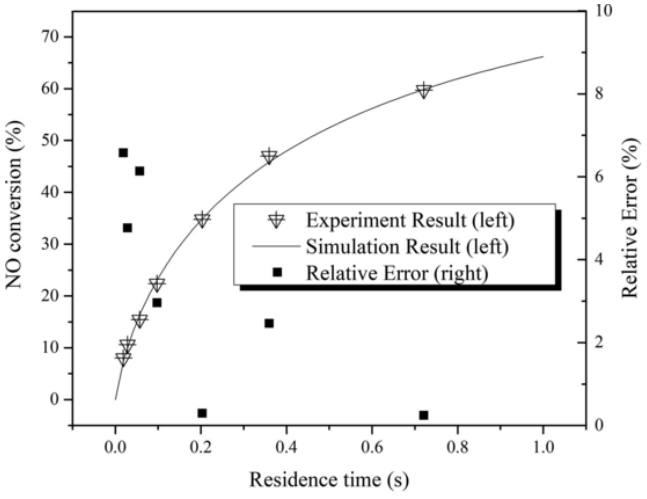


**Fig. 7.** Comparison between experimental results according to Ref. [46] and simulation results in this work. Variation of conversion rate of NO decomposition with residence time between catalysts and gas is shown.

might be that NO decomposition reaction becomes more significant as residence time increases, which can benefit the measurement of reactants and products. The measurement error thereby decreases and experimental results are close to the simulation results, which contributes to lower relative error.

#### 4.1.2. Solar-aided power generation model

To ensure the accuracy of SAPG model, results obtained from the model are compared with the results from literature [49,51], where the model assumes that flue gas transfers no heat to feed water. Key parameters of the 600 MW coal-fired power plant are given in Table 3. The comparison results are shown in Table 4. The relative errors between the model and the literature are below 3%, which indicates that the calculation model is reliable. The error might be caused by the calculation differences of thermodynamic parameters of water and steam.

**Table 3**
Key parameters of a 600 MW coal-fired power plant.

| Item | Unit | Designed data | Simulated Results | Relative Error |
|---|---|---|---|---|
| Power | MW | 600 | 600 | 0.00% |
| Steam Pressure | MPa | 16.7 | 16.7 | – |
| Steam Temperature | ˚C | 537 | 537 | – |
| Specific Enthalpy of Superheated Steam | kJ/kg | 3394.4 | 3395.783 | 0.041% |
| Reheated Steam Temperature | ˚C | 537 | 537 | – |
| Specific Enthalpy of Reheated Steam | kJ/kg | 3536.6 | 3537.995 | 0.039% |
| Mass Flow Rate of Reheated Steam | Kg/s | 513.567 | 512.697 | 0.169% |
| Exhausted steam pressure | kPa | 4.5/5.39 | 4.5/5.39 | – |
| Exhausted steam enthalpy | kJ/kg | 2333.8 | 2333.8 | – |

### 4.2. Performances of NO decomposition

After the pretreatment of flue gas, there are mainly four compositions, including $CO_2$, $O_2$, $N_2$ and a small amount of $NO_x$ as listed in Table 2. In the chemical kinetics model, $NO_2$ accounts for no more than 10% of $NO_x$ [4], and it is considered to be one of the reactants for $O_2$ and NO formation ($O^* + NO_2 \Leftrightarrow NO_3^*$, $NO_3^* \Leftrightarrow O_2^* + NO$ and $O_2^* \Leftrightarrow O_2 + *$) [46] in NO decomposition. Thus we regard volume fraction of $NO_x$ as that of NO. The reaction of NO decomposition is based on Cu-ZSM-5 catalyst.

Conversion rate of NO decomposition is one of the most important parameters. Its variation with temperature and residence time is shown in Fig. 8. Although NO decomposition is thermodynamically favorable, its kinetics is slow, because the concentration of NO in the flue gas is extremely low and the concentration of $O_2$ is relatively high. Thus, analysis of kinetics of the reaction presents more importance than its thermodynamics. In Fig. 8(a), the conversion rate of NO decomposition increases with the residence time. The conversion rate increases rapidly up to approximately 70%-80% in 100 s, while its growth gradually slows down after 100 s. The reason might be that the concentration of NO decreases and the concentration of $O_2$ increases as the reaction progresses which reduces the decomposition rate as described in Eq. (4). The equation with second-order NO dependencies would be very sensitive to the concentration of NO, which contributes to the rapid growth at the beginning stage.

The conversion rate is also related to the temperature of reactants, which can be clearly seen in Fig. 8(b). The maximum value of each curve is in the range of 480–510 ˚C, which means that the conversion rate of NO decomposition increases with temperature to the maximum, and then decreases. Luckily, the temperature range is within the safety range (< 550 ˚C) [33] of PTC, which makes it possible to heat flue gas to the optimal temperature range. To make the volume fraction of NO below 100 ppm after NO decomposition, the conversion rate is required

**Table 4**
Comparison results between the model and the literature [49,51].

| Item | | Unit | FWH1 | FWH2 | FWH3 | FWH4 | FWH5 | FWH6 | FWH7 | FWH8 |
|---|---|---|---|---|---|---|---|---|---|---|
| Extraction Pressure | Design data | MPa | 5.894 | 3.5931 | 1.6122 | 0.7447 | 0.3054 | 0.1301 | 0.0698 | 0.022 |
| | Simulation Results | MPa | 5.894 | 3.5931 | 1.6122 | 0.744 | 0.3054 | 0.1301 | 0.0698 | 0.022 |
| | Error | MPa | – | – | – | – | – | – | – | – |
| Enthalpy of Extraction Steam | Design data | kJ/kg | 3132.9 | 3016 | 3317.7 | 3108.2 | 2912.9 | 2749.5 | 2649.5 | 2491.1 |
| | Simulation Results | kJ/kg | 3134.0 | 3017.0 | 3317.7 | 3108.2 | 2912.9 | 2749.5 | 2649.5 | 2491.1 |
| | Error | kJ/kg | 1.1 | 1.0 | 0.0 | 0.0 | 0.0 | 0.0 | 0.0 | 0.0 |
| Extraction Coefficient of Steam | Design data | | 0.07289 | 0.08286 | 0.03833 | 0.04180 | 0.03497 | 0.02203 | 0.03402 | 0.03058 |
| | Simulation Results | | 0.07296 | 0.08109 | 0.04000 | 0.04168 | 0.03501 | 0.02205 | 0.03392 | 0.03064 |
| | Relative Error | % | 0.096 | 2.183 | 0.417 | 0.288 | 0.114 | 0.091 | 0.295 | 0.196 |
| Outlet Temperature of Feed water | Design data | ˚C | 274.1 | 242.3 | 199.3 | 165.4 | 129.6 | 102.9 | 85.7 | 58.2 |
| | Simulation Results | ˚C | 274.15 | 242.32 | 200.28 | 165.38 | 129.59 | 102.84 | 85.71 | 58.21 |
| | Error | ˚C | 0.05 | 0.02 | 0.98 | −0.02 | −0.01 | −0.06 | 0.01 | 0.01 |
| Enthalpy of Drain Water | Design data | kJ/kg | 1075.4 | 874.9 | 737.5 | 699.3 | 454.8 | 382.5 | 267 | 161.9 |
| | Simulation Results | kJ/kg | 1075.12 | 879.18 | 737.97 | 699.01 | 454.44 | 382.08 | 266.73 | 160.28 |
| | Error | kJ/kg | −0.28 | 4.28 | 0.47 | −0.29 | −0.36 | −0.42 | 0.73 | −1.62 |

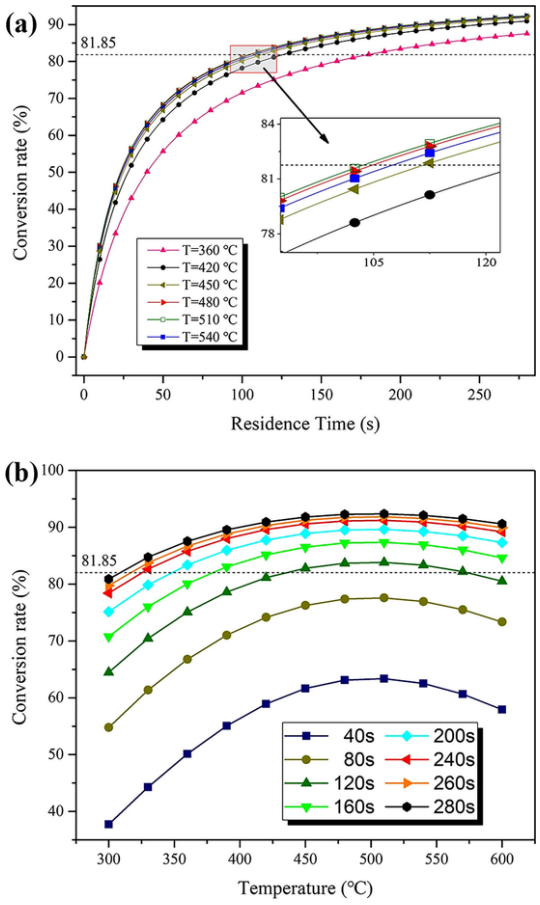


**Fig. 8.** Effect of temperature on chemical kinetics of NO decomposition at 1 bar; (a) variation of the conversion rate with residence time at different temperatures; (b) variation of the conversion rate with temperature at different residence time.

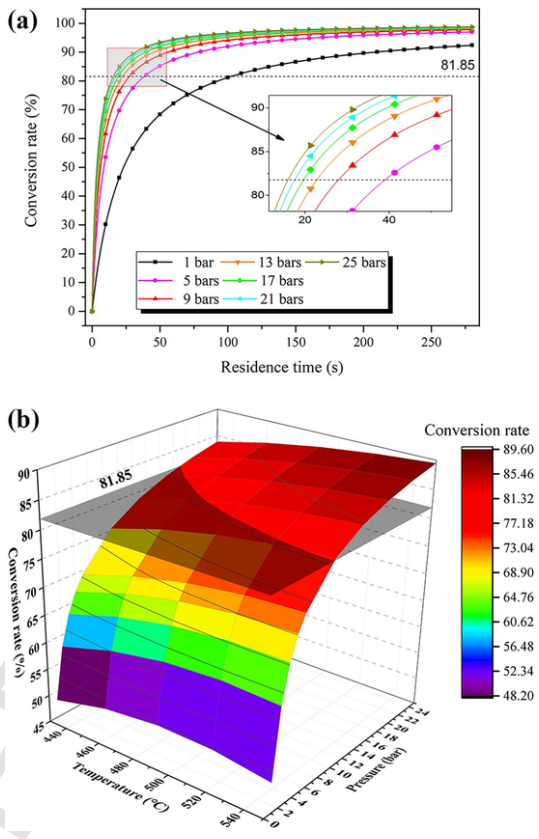


**Fig. 9.** Effect of pressure on chemical kinetics of NO decomposition: (a) variation of the conversion rate with residence time at 490 °C and different pressure; (b) variation of the conversion rate with both temperature and pressure, at a residence time of 25 s.

more than 81.85%. And the curves above the dotted line, which are corresponding to the value more than 81.85 on y-axis, mean that the conversion rate is higher than 81.85% and the concentration of NO is below 100 ppm.

In Fig. 9(a), the conversion rate of NO decomposition increases with pressure. The result can be explained that the concentration of NO increases with the pressure (see Eq. (2)). Although the concentration of $O_2$ also increases with pressure which will reduce the decomposition rate according to Eq. (4), its effect is much less than NO for the equation with second-order NO dependencies. The curves at pressures of 5–24 bars rise rapidly up to nearly 85%-95% within a residence time of 50 s, whose growth rates are much larger than that at 1 bar (see Fig. 9a). In such cases, increasing the pressure can effectively promote the decomposition reaction. Nevertheless, the effect of this method is getting weaker as the pressure increases, since the curves are getting closer to each other at a pressure of more than 5 bars.

The effect of both temperature and pressure on the conversion rate is presented as Fig. 9(b). It could be found that the conversion rate increases as temperature (or pressure) rises. The translucent black plane corresponds to the value of 81.85 on the z-axis, above which the conversion rate is higher than 81.85% and the concentration of NO is lower than 100 ppm. Considering that flue gas might be at a high pressure and a high temperature, we could fully utilize this advantage to accelerate the chemical kinetics.

### 4.3. Performances of SAGT & SAPG

Fig. 10 shows the variation of SEE with DNI. It can be clearly seen that SEE increases as DNI varies in a range of 200–900 W/m$^2$. The reason might be that heat losses become smaller as DNI increases, which can be known from Eq. (B.1). When DNI is greater than 500 W/m$^2$, SEE increases more and more slowly. In the range from 500 W/m$^2$ to 900 W/m$^2$, the total SEE increases by no more than 1.5% in a temperature range from 300 °C to 550 °C and the maximal value of SEE increases by about 1%, as shown in Fig. 10(a) and (b). In addition, the maximal values of SEE are all higher than 22.5%. Therefore, SEE has a relatively good stability as well as a high performance when DNI is higher than 500 W/m$^2$. In the other hand, SEE shows relatively bad performances when DNI is below 400 W/m$^2$, which is a common problem among solar-aided coal-fired power plant systems. The disadvantage is still acceptable, because the advantages of SAPG is more prominent. Moreover, the concept has advantages not only in the aspect of SAPG, but also SAGT.

Fig. 11 shows the results of SAGT and SAPG together, which directly reflects the main improvement of the advanced concept. It can be clearly seen that the temperatures corresponding to the maximal values of both curves are close to 500 °C which is within the safety range of PTC (< 550 °C). If the volume fraction of $NO_x$ is desired to be less than 100 ppm, conversion rate of NO decomposition is required to be larger than 81.85%. This requires that the temperature should be higher than 358 °C. Thereby the operation temperature has a wide range between 358 °C and 550 °C, and the difference between these two temperatures reaches up to 192 °C. This means that, even if the temperature fluctuations caused by unfavorable factors such as fluctuations of DNI or con-

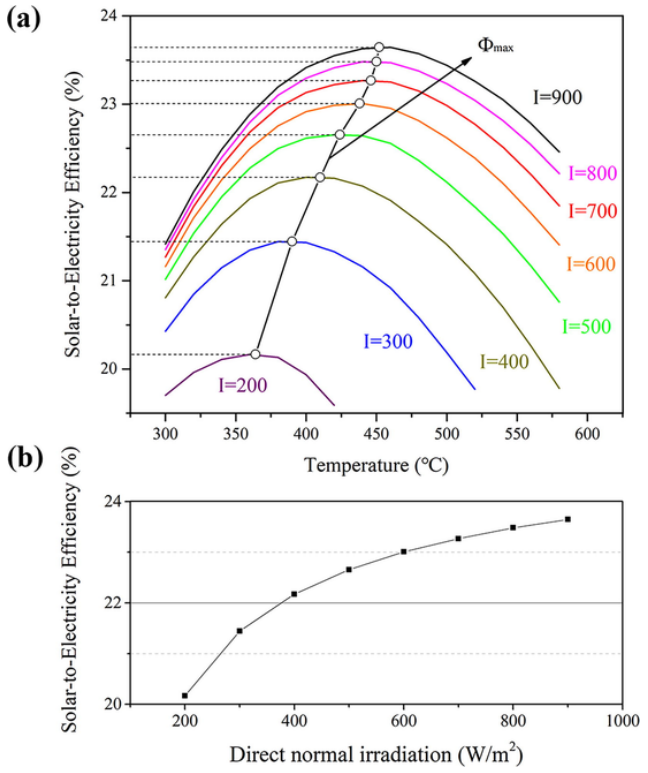


**Fig. 10.** Effect of DNI on solar-to-electricity efficiency (SEE): (a) variation of SEE with temperature, corresponding to different DNI ranging from 200 to 900 W/m$^2$; (b) variation of the maximal value of SEE for each curve with DNI.

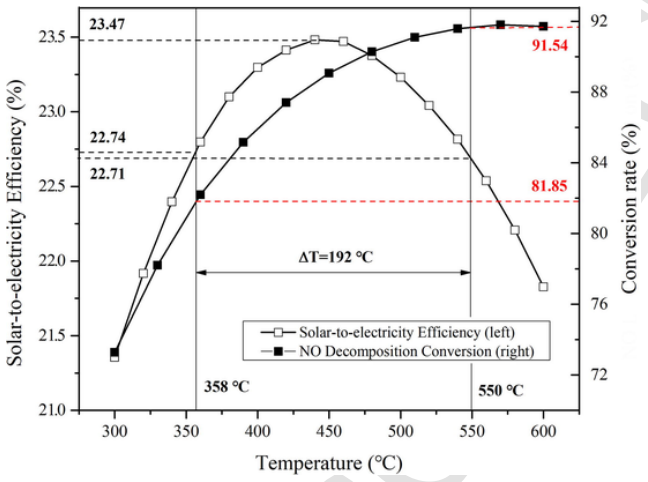


**Fig. 11.** Variation of solar-to-electricity efficiency (SEE) and conversion rate of NO decomposition with flue gas temperature. The curve of SEE is based on DNI at 800 W/m$^2$, while the curve of conversion rate is at the pressure of 9 bars and residence time of 60 s.

trol delay, SAGT part can operate normally as long as it is within this temperature range (358–550 °C). SAGT part shows a high conversion rate from 81.85% to 91.54%. Furthermore, SAPG part also shows a splendid performance with a SEE between 22.71% and 23.47% in the temperature range between 358 °C and 550 °C.

As shown in Fig. 12, curves under different conditions almost satisfy the similar rules presented in Fig. 11. The maximal value of the curve of SEE at DNI of 500 W/m$^2$ deviates significantly from 500 °C. However, the temperature ranges of high performances of both SEE and NO decomposition still have a good match with each other, and the maximal values of these curves are almost within the orange region. The results show that coupling SAGT and SAPG has relatively good compatibility and stability.

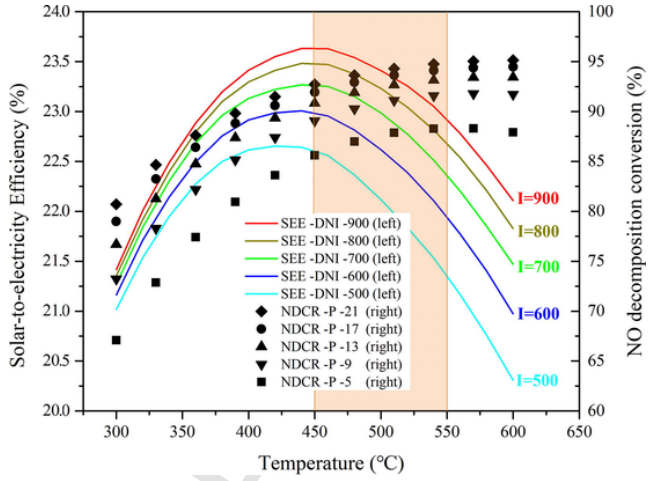


**Fig. 12.** Variation of solar-to-electricity efficiency (SEE) and conversion rate of NO decomposition with flue gas temperature. The curve of SEE is at different DNIs ranging from 500 W/m$^2$ to 900 W/m$^2$, while the curve of NO decomposition conversion rate (NDCR) is at different pressures ranging from 5 bars to 21 bars and a residence time of 60 s.

The above results are based on design conditions of both the solar part and the power plant. Considering the situations of coupling SAGT & SAPG with existing power plants, off-design performances of this concept are necessary. Fig. 13(a) shows the off-design performance of SAGT & SAPG, from which reduced SEE can be observed by comparing with the design conditions. The reason might be the deviation of the turbine from the optimum condition when solar energy is integrated with the power plant. Reducing extraction steam makes the turbine overloaded, which leads to a relatively low efficiency enhancement. Thus, SEE performance at off-design conditions is worse than that at design conditions. From Fig. 13(b), an interesting result can be observed that a low unit load corresponds to high SEE. When reducing the working load, the power plant would be at an off-design condition. The overall efficiency of the power plant would be decreased, which means that working at 50% load needs more than 50% coal of 100% load. Calculation results has also confirmed this conclusion. The amount of flue gas is proportion to the amount of burned coal. When the temperature of flue gas treatment is designed, the heat required from solar energy is also proportion to the amount of burned coal. Therefore, the share of solar energy introduced in the power plant would increase as the working load decreases. More high pressure feed water heaters as well as other extraction steam are thereby replaced. As shown in Fig. 13(b), the substitution of extraction steam is presented. More stages of extraction steam can be substituted in lower working load (from high pressure extraction steam to low pressure extraction steam). It contributes to a much higher overall efficiency of the power plant. Moreover, the load of turbine is lower than the rated working condition. Reducing the extraction steam can increase its load and make it more close to the rated working condition. Both of them might be the reasons why a low unit load corresponds to high SEE.

## 5. Conclusion

In summary, an advanced concept of coupling SAGT and SAPG outside boilers for power plants has been proposed. Results show that higher temperature and larger gas pressure contribute to faster kinetics, and higher DNI is beneficial for SEE. It is desired for the conditions such as catalysts with faster kinetics, operation conditions with larger gas pressure, higher temperature and larger DNI. In addition, NO de-

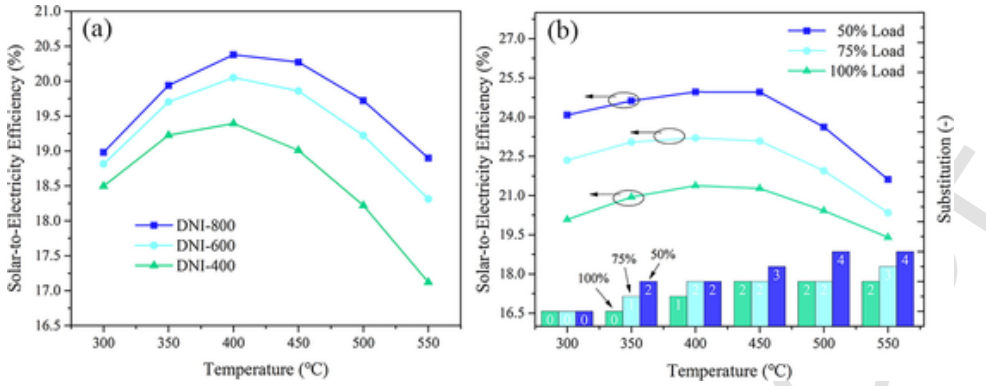


**Fig. 13.** Variation of solar-to-electricity efficiency (SEE) with flue gas temperature in off-design conditions, including: a) the curve of SEE at different DNIs of 400, 600 and 800 W/m$^2$; b) the curve of SEE corresponding to different working conditions at the DNI of 800 W/m$^2$, and the number of stages of extraction steam which can be substituted.

composition technology might become another competitive $NO_x$ control technology because it consumes no reducing agent.

The concept provides a new way of utilizing solar energy for both energy conservation and environmental protection. An improved flue gas treatment sequence is proposed to make it possible for flue gas treatment outside boilers. It could also help to protect catalysts and devices from damage. The concept might be applied not only to coal-fired power plants, but also to other heavy polluting industries such as steel plants, coking plants, cement plants, fertilizer plants and various chemical plants where solar thermal energy could be utilized for heat recovery after flue gas treatment.

## Declaration of Competing Interest

The authors declare that they have no known competing financial interests or personal relationships that could have appeared to influence the work reported in this paper.

## Acknowledgements

This study was supported by the National Key Research and Development Program of China (2016YFB0901401), the National Natural Science Foundation under award number (51676189) and the Chinese Academy of Sciences Frontier Science Key Research Project under award number (QYZDY-SSW-JSC036).

## Appendix A.

This Appendix presents the combustion calculation of fuel in order to obtain the molar ratio of the components in flue gas.

In the combustion process, NO can be divided into three types: thermal NO, prompt NO and fuel NO. Among them, 75–95% of the total NO generated originates from fuel-bound nitrogen with prompt NO accounting no more than 5% of the total NO [9]. Mass of fuel NO would be calculated as [52]:

$$\widetilde{G}_{NO} = 1.63B(\beta \cdot N + 10^{-6} V_y \cdot C_{NO}) \tag{A.1}$$

where $\widetilde{G}_{NO}$ is the mass of NO, kg; $B$ is the mass of fuel such as coal ($B$ is assigned as a value of 1 in this calculation), kg; $\beta$ is the conversion of nitrogen to NO which is generally in a range of 15%–40%, and it is assigned as a value of 25% [9]; $N$ is the percentage content of nitrogen in fuel, which can be obtained in Table 1. $V_y$ is the volume of flue gas produced by 1 kg of fuel, Nm$^3$ /kg; $C_{NO}$ represents the concentration of thermal NO that is produced in high temperature ($C_{NO}$ usually is 93.8 mg/Nm$^3$), mg/Nm$^3$.

Theoretical air that is consumed by 1 kg of coal is calculated as [53]:

$$\widetilde{n}_{TA} = \frac{\widetilde{m}_{TA}}{M_{air}} = \frac{1000}{M_{air}} \left\{ 11.51C + 34.3 * \left( H - \frac{O}{7.94} \right) + 4.31S \right\} /100 \tag{A.2}$$

where $\widetilde{n}_{TA}$ is the amount of substance of theoretical air, mol/kg coal; $\widetilde{m}_{TA}$ is the mass of theoretical air, g/kg coal; $M_{air}$ represents relative molecular mass of air which is defined as 29 g/mol. C, H, O, S represent percentage contents of carbon, hydrogen, oxygen, sulfur, respectively, as listed in Table 1.

The equations utilized to calculate the amounts of substance of $NO_x$, $CO_2$, $O_2$ and $N_2$ per kg of coal are provided as follows:

$$\widetilde{n}_{NOx} = \frac{1}{0.9} \cdot \widetilde{n}_{NO} = 1000 \cdot \frac{1}{0.9} \cdot \frac{\widetilde{G}_{NO}}{30} \tag{A.3}$$

$$\widetilde{n}_{CO_2} = 1000 \cdot \frac{C}{12} \cdot \frac{1}{100} \tag{A.4}$$

$$\widetilde{n}_{O_2} = 0.21 \cdot (\alpha_{ex} - 1) \cdot \widetilde{n}_{TA} \tag{A.5}$$

$$\widetilde{n}_{N_2} = 0.79 \cdot \alpha_{ex} \cdot \widetilde{n}_{TA} + 1000 \cdot \frac{N}{14} \cdot \frac{1}{100} - \widetilde{n}_{NOx} \tag{A.6}$$

where $\widetilde{n}_{NOx}$, $\widetilde{n}_{CO_2}$, $\widetilde{n}_{O_2}$, $\widetilde{n}_{N_2}$ are amounts of substance of $NO_x$, $CO_2$, $O_2$ and $N_2$, respectively, mol/kg coal; $\alpha_{ex}$ is excess air ratio, $\alpha_{ex}$ is chosen as 1.2.

## Appendix B.

This Appendix presents the calculation details of solar collector efficiency.

Considering the losses of absorbed solar energy incident on the collector, the solar collector efficiency ($\eta_{col}$) is given as [54]:

$$\eta_{col} = k \cdot (73.3 - 0.007276 \cdot \Delta T) - 0.496 \cdot \left( \frac{\Delta T}{I} \right) - 0.0691 \cdot \left( \frac{\Delta T^2}{I} \right) \tag{B.1}$$

where $\Delta T$ represents the difference between ambient temperature ($T_{amb}$) and the average temperature ($T_{ave}$) of solar field, K. The average temperature of solar collector ($T_{ave}$) is expressed as Eq. (B.2):

$$T_{ave} = \frac{T_{sfield,\,i} + T_{sfield,\,o}}{2} \tag{B.2}$$

where $T_{sfield,i}$ represents the temperature of flue gas in the inlet of solar field, K; $T_{sfield,o}$ is the temperature of flue gas in the outlet of solar field, K; $k$ in the Eq. (B.1) represents the incidence angle correction factor

which is expressed as:

$$k = \cos\theta - 0.0003512\cdot\theta - 0.00003137\cdot\theta^2 \quad \text{(B.3)}$$

where $\theta$ is incidence angle (here $\theta$ is assigned as 0°).

## Appendix C.

This Appendix presents the calculation details of heat exchangers between high temperature flue gas and feed water.

The ratio of the heat transferred from flue gas to feed water to the enthalpy drop of flue gas in heat exchanger ($\eta_{exc}$) is expressed as follows:

$$\eta_{exc} = 1 - \eta_{loss} \quad \text{(C.1)}$$

$$\eta_{loss} = \frac{\dot{Q}_{loss}}{\Delta\widetilde{h}_{fg,\,n}} \times 100\% \quad \text{(C.2)}$$

$$\widetilde{Q}_{loss} = h\cdot A_{wall}\cdot\left(T_{wall} - T_{amb}\right) + \varepsilon\cdot\sigma\cdot\left(T_{wall}^4 - T_{amb}^4\right) \quad \text{(C.3)}$$

where $\eta_{loss}$ is the ratio of losses of heat to the enthalpy drop of flue gas, $\Delta\widetilde{h}_{fg,\,n}$, when heat is transferred from flue gas to feed water in the heat exchangers, %; $\widetilde{Q}_{loss}$ is the heat losses from heat exchangers, kJ/kg coal; $h$ is convective heat transfer coefficient, kW/(m$^2$·K); $A_{wall}$ represents the area of the outer surface of the insulating layer outside the heat exchanger, m$^2$; $\varepsilon$ is the emissivity of the outer surface of the insulating layer; $\sigma$ is Stefan-Boltzmann constant, $5.67 \times 10^{-8}$ W/(m$^2$·K$^4$); $T_{wall}$ is the temperature of the outer surface of the insulating layer, K, which depends on the material and thickness of insulating layer; $T_{amb}$ is ambient temperature, 297.15 K. Given that lower heat transfer coefficient and thicker insulating layer contributes to less heat losses, here $\eta_{loss}$ is assumed as 5% for simplification of the calculations.

# Footnotes

## Article Footnotes

## Text Footnotes

## References


[1] International Energy Agency. Electricity information: Overall; 2018.
[2] China Statistical Publishing House. China Statistic Yearbook; 2018.
[3] S Liu, Z Zhang, Y Wang, Y Hu, W Liu, C Chen, et al. PM2.5 emission characteristics of coal-fired power plants in Beijing-Tianjin-Hebei region, China. Atmos Pollut Res 2019;10:954–959.
[4] Q Sun, Z Wang, D Wang, Z Hong. A review on the catalytic decomposition of NO to $N_2$ and $O_2$---catalysts and processes. Catal Sci Technol 2018.
[5] B He, C Chen. Energy ecological efficiency of coal fired plant in China. Energy Convers Manage 2002;43:2553–2567.
[6] P Breeze. Chapter 4 - combustion plant emissions: sulfur dioxide, nitrogen oxides, and acid Rain. In: P Breeze, editor. Electricity generation and the environment. Academic Press; 2017. p. 33–47.
[7] HN Soud, SC Mitchell. Particulate control handbook for coal-fired plants. IEA Coal Research; 1997.
[8] BG Miller. Chapter 8 - Advanced flue gas dedusting systems and filters for ash and particulate emissions control in power plants. In: D Roddy, editor. Advanced power plant materials, design and technology. Woodhead Publishing; 2010. p. 217–243.
[9] BG Miller. Chapter 9 - emissions control strategies for power plants. In: BG Miller, editor. Clean coal engineering technology. Boston: Butterworth-Heinemann; 2011. p. 375–481.
[10] HN Soud. Developments in FGD. IEA Coal Research; 2000.
[11] B Dou, W Pan, Q Jin, W Wang, Y Li. Prediction of SO2 removal efficiency for wet Flue Gas Desulfurization. Energy Convers Manage 2009;50:2547–2553.
[12] Environment Protection Agency. Technical Bulletin, Nitrogen Oxides (NOx), Why and How They Are Controlled. In: O.o.A.Q.P.a. Standards, editor. U. S. Government Printing Office; November, 1999.
[13] Environment Protection Agency. Performance of Selective Catalytic Reduction on Coal-Fired Steam Generating Units. In: O.o.A.a. Radiation, editor. U. S. Government Printing Office; June 25, 1997.
[14] Department of Energy. Clean Coal Technology, Control of Nitrogen Oxide Emissions: Selective Catalytic Reduction (SCR), Topical Report Number 9. In: U.S.D.o. Energy, editor. July, 1997.
[15] Y Shi, S Tan, X Wang, M Li, S Li, W Li. Regeneration of sulfur-poisoned CeO2 catalyst for NH3-SCR of NOx. Catal Commun 2016;86:67–71.
[16] Z Wu. NOx control for pulverized coal fired power stations. IEA Coal Research; 2002.
[17] J Sun, R Wang, H Hong, Q Liu. An optimized tracking strategy for small-scale double-axis parabolic trough collector. Appl Therm Eng 2017;112:1408–1420.
[18] S Tang, H Hong, J Sun, W Qu. Efficient path of distributed solar energy system synergetically combining photovoltaics with solar-syngas fuel cell. Energy Convers Manage 2018;173:704–714.
[19] Y Han, C Xu, G Xu, YW Zhang, YP Yang. An improved flexible solar thermal energy integration process for enhancing the coal-based energy efficiency and NOx removal effectiveness in coal-fired power plants under different load conditions. Energies 2017;10:1485–1502.
[20] RJ Zoschak, SF Wu. Studies of the direct input of solar energy to a fossil-fueled central station steam power plant. Sol Energy 1975;17:297–305.
[21] LV Griffith, H Brandt. Solar-fossil HYBRID system analysis: performance and economics. Sol Energy 1984;33:265–276.
[22] E Hu, Y Yang, A Nishimura, F Yilmaz, A Kouzani. Solar thermal aided power generation. Appl Energy 2010;87:2881–2885.
[23] J Qin, E Hu, GJ Nathan. The performance of a Solar Aided Power Generation plant with diverse "configuration-operation" combinations. Energy Convers Manage 2016;124:155–167.
[24] J Qin, E Hu, GJ Nathan. Impact of the operation of non-displaced feedwater heaters on the performance of Solar Aided Power Generation plants. Energy Convers Manage 2017;135:1–8.
[25] Y Yang, Q Yan, R Zhai, A Kouzani, E Hu. An efficient way to use medium-or-low temperature solar heat for power generation – integration into conventional power plant. Appl Therm Eng 2011;31:157–162.
[26] MVJJ Suresh, KS Reddy, AK Kolar. 4-E (Energy, Exergy, Environment, and Economic) analysis of solar thermal aided coal-fired power plants. Energy Sustainable Dev 2010;14:267–279.
[27] R Zhai, C Li, Y Chen, Y Yang, K Patchigolla, JE Oakey. Life cycle assessment of solar aided coal-fired power system with and without heat storage. Energy Convers Manage 2016;111:453–465.
[28] J Wu, H Hou, Y Yang, E Hu. Annual performance of a solar aided coal-fired power generation system (SACPG) with various solar field areas and thermal energy storage capacity. Appl Energy 2015;157:123–133.
[29] J Wu, H Hou, Y Yang. Annual economic performance of a solar-aided 600MW coal-fired power generation system under different tracking modes, aperture areas, and storage capacities. Appl Therm Eng 2016;104:319–332.
[30] J Li, Z Wu, K Zeng, G Flamant, A Ding, J Wang. Safety and efficiency assessment of a solar-aided coal-fired power plant. Energy Convers Manage 2017;150:714–724.
[31] R Wang, J Sun, H Hong, H Jin. Comprehensive evaluation for different modes of solar-aided coal-fired power generation system under common framework regarding both coal-savability and efficiency-promotability. Energy 2018;143:151–167.

[32] RG Patil, SV Panse, JB Joshi. Optimization of non-evacuated receiver of solar collector having non-uniform temperature distribution for minimum heat loss. Energy Convers Manage 2014;85:70–84.
[33] M. Eck, N. Benz, J.F. Feldhoff, Y. Gilon, Z. Hacker, T. Müller, et al. The potential of direct steam generation in parabolic troughs – Results of the German Project DIVA. In: P.o.t.t.B.C.S. Symposium, editor. Las Vegas, USA; 2008.
[34] İ Yılmaz, MS Söylemez. Thermo-mathematical modeling of parabolic trough collector. Energy Convers Manage 2014;88:768–784.
[35] M Tortorelli. Innovative technology for NOx direct decomposition. University Of Naples Federico II; 2014.
[36] VI Pârvulescu, P Grange, B Delmon. Catalytic removal of NO. Catal Today 1998;46:233–316.
[37] F Garin. Mechanism of NOx decomposition. Appl Catal A 2001;222:183–219.
[38] M Iwamoto, H Furukawa, S Kagawa. Catalytic decomposition of nitric monoxide over copper ion-exchanged zeolites. In: Y Murakami, A Iijima, JW Ward, editors. Studies in surface science and catalysis. Elsevier; 1986. p. 943–949.
[39] M Iwamoto. Chapter II.3 catalytic decomposition of nitrogen monoxide. In: M Misono, Y Moro-oka, S Kimura, editors. Studies in Surface Science and Catalysis. Elsevier; 1990. p. 121–143.
[40] N Imanaka, T Masui. Advances in direct NOx decomposition catalysts. Appl Catal A-Gen 2012;431:1–8.
[41] C Tofan, D Klvana, J Kirchnerova. Decomposition of nitric oxide over perovskite oxide catalysts: effect of CO2, H2O and CH4. Appl Catal B-Environ 2002;36:311–323.
[42] B Heidel, M Hilber, G Scheffknecht. Impact of additives for enhanced sulfur dioxide removal on re-emissions of mercury in wet flue gas desulfurization. Appl Energy 2014;114:485–491.
[43] J Bugge, S Kjær, R Blum. High-efficiency coal-fired power plants development and perspectives. Energy 2006;31:1437–1445.
[44] J Wu, H Hou, Y Yang. The optimization of integration modes in solar aided power generation (SAPG) system. Energy Convers Manage 2016;126:774–789.
[45] Z Ouyang, J Zhu, Q Lu. Experimental study on preheating and combustion characteristics of pulverized anthracite coal. Fuel 2013;113:122–127.
[46] B Modén, P Da Costa, B Fonfé, DK Lee, E Iglesia. Kinetics and mechanism of steady-state catalytic NO decomposition reactions on Cu–ZSM5. J Catal 2002;209:75–86.
[47] NIST chemistry webbook. U. S. Department of Commerce, https:// webbook. nist.gov/ chemistry/fluid/; 2018 [accessed 20 May 2018].
[48] D Che. Boilers: theory, design and operation. Xi'an Jiaotong University Press; 2008.
[49] X Huang. Curriculum design of thermal power plant. China Electric Power Press; 2004.
[50] C Li, R Zhai, Y Yang, K Patchigolla, JE Oakey. Thermal performance of different integration schemes for a solar tower aided coal-fired power system. Energy Convers Manage 2018;171:1237–1245.
[51] H Hou, Z Xu, Y Yang. An evaluation method of solar contribution in a solar aided power generation (SAPG) system based on exergy analysis. Appl Energy 2016;182:1–8.
[52] P Fang, X Jiang, Y Xi. Handbook of environmental statistics. China: Sichuan Science & Technology Press Sichuan; 1985.
[53] DK Sarkar. Chapter 3 - fuels and combustion. In: DK Sarkar, editor. Thermal power plant. Elsevier; 2015. p. 91–137.
[54] D. VE, K. GJ, M. AR. Test results: SEGS LS-2 solar collector. NASA STI/Recon technical report N, 1994.